Redox-driven changes in water-dispersible colloids and their role in carbon cycling in hydromorphic soils

Redox-driven changes in water-dispersible colloids and their role in carbon cycling in hydromorphic soils

Daniel Said-Pullicino[1], Beatrice Giannetta[1], Beatrice Demeglio[1], Anna Missong[2], Nina Gottselig[3], Marco Romani[4], Roland Bol[2], Erwin Klumpp[2], Luisella Celi[1]

[1]*Soil Biogeochemistry, Department of Agricultural, Forest and Food Sciences, University of Torino, Grugliasco (TO), Italy.*

[2]*Institute of Bio- and Geosciences, Agrosphere Institute (IBG-3), Forschungszentrum Jülich, Germany.*

[3]*Soil Science and Soil Ecology, Institute of Crop Science and Resource Conservation, Universität Bonn, Germany.*

[4]*Rice Research Centre, Ente Nazionale Risi, Castello d'Agogna, Italy.*

Abstract

Redox fluctuations in hydromorphic soils can influence ecosystem functions by altering the cycling of organic carbon (OC) and other elements in both the aqueous and solid phases throughout the soil profile. Most studies focusing on the mobility of dissolved OC in rice paddy soils have often disregarded the contribution of colloidal particles. We provide a detailed chemical and size-related characterization of water-dispersible soil colloids and their depth distribution in two soil profiles under long-term temperate paddy and non-paddy management, by asymmetric flow field-flow fractionation. Anoxic conditions enhanced colloid dispersion with a preferential release of the finer colloid fractions (5 and 4-fold increase in the < 30 nm and 30-240 nm fractions, respectively). The mobility of OC-rich, iron and aluminium (hydr)oxide and aluminosilicate colloids along the soil profile was probably responsible for their depletion in the topsoil and a corresponding accumulation in the deeper illuvial horizons compared to the non-paddy soil. However, the release, percolation and subsequent reoxidation of Fe^{2+} was also shown to be a plausible mechanism leading to the formation of fine colloids in the subsoil. Redox-driven changes in colloid distribution were also linked to the differences in OC and pedogenetic iron stocks in these two agro-ecosystems.

Keywords: Rice paddy soils, water-dispersible fine colloids, asymmetric flow field-flow fractionation, Fe (hydr)oxides, organic C stocks, subsoil.

INTRODUCTION

Paddy soils are not only important soil resources for sustaining global food security through rice production, but also constitute the largest anthropogenic wetland with key ecosystem functions (Kögel-Knabner et al., 2010). They represent a major terrestrial carbon (C) pool, storing a large proportion of the global terrestrial C stocks (*ca.*10 Pg) (Kirk, 2004). Paddy management, which often involves rice monocropping in flooded paddies with one, two or even three cropping cycles per year and may include the incorporation of large amounts of crop residues, strongly affects the organic carbon (OC) turnover, hydrology and redox chemistry of these soils (Kögel-Knabner et al., 2010). Although the greater soil OC accumulation rates in paddy topsoils with respect to non-paddy soils is generally assumed to be due to limited mineralization under anoxic soil conditions resulting from frequent field flooding (Cheng et al., 2009), there is growing evidence questioning this assumption (Huang and Hall, 2017).

Organic matter (OM) turnover and stabilization in redoximorphic soils are strongly linked to the dynamic interactions with redox-active minerals, in particular iron (Fe) oxyhydroxides (hereafter referred to as Fe oxides), that may provide mineral surfaces for OC protection or act as electron acceptors for microbial OC mineralization under anoxic conditions (Buettner et al., 2014; Hall et al., 2018; Huang and Hall, 2017; Huang et al., 2020). The reductive dissolution of Fe oxides under anoxic conditions may release associated dissolved organic C (DOC) into solution, that may be subsequently mineralized (Dunham-Cheatham et al., 2020), retained by adsorption and coprecipitation during the formation of Fe(III) phases when oxic conditions are re-established (Mikutta et al., 2014; Sodano et al., 2017), or transported into deeper mineral horizons through percolation (Katoh et al., 2004; Maie et al., 2004; Said-Pullicino et al., 2016). Various studies have evidenced that most OC accumulation under paddy management is restricted to the puddled layer, as the presence of a dense plough pan prevents OC from entering deeper soil layers (Kalbitz et al., 2013; Roth et al., 2011; Wissing et al., 2011; Wissing et al., 2014). However, DOC fluxes in temperate paddy soils under continuous flooding reported by Said-Pullicino et al. (2016) suggest substantial OC inputs into the subsoil in these poorly-developed, coarse-textured soils.

Although the contribution of subsoil OC contents to total C stocks is well-recognized (Rumpel and Kögel-Knabner, 2011; Scharlemann et al., 2014), information on the processes controlling OC mobility and transport in paddy soils under long-term submerged rice cultivation remains scarce. Considering that the persistence of OC in deeper mineral horizons can be ascribed to the association with soil minerals, particularly short-range-ordered (SRO)

metal oxides (Chorover et al., 2004; Kramer et al., 2012; Lalonde et al., 2012; Mikutta et al., 2009), further insights into the effects of redox alternations on Fe phase composition, crystal order and depth distribution, as well as the link to the turnover of mineral-associated OM, are necessary. Most studies on DOC mobility under paddy management have focused on OC fractions < 450 nm, even though both dissolved and particulate OC can constitute this fraction and have been recognized as important vehicles for C transport (Marin-Spiotta et al., 2011). Soil colloids have been reported to play an important role in determining transport properties of various elements including OC, phosphorus (P), Fe, aluminium (Al), silicon (Si), and trace metals across different ecosystems, including grassland (Henderson et al., 2012; Jiang et al., 2017), forest (Buettner et al., 2014; King et al., 2019; Missong et al., 2018; Wang et al., 2020) and agricultural lands (Jiang et al., 2015). Studies on the role of colloids in element cycling in rice paddies has been limited to the evaluation of organo-mineral associations in water-dispersible colloids in paddy topsoils as a function of management practices (Huang et al., 2020), or to the quantification of colloid-facilitated migration of P with surface runoff and along the soil profile as affected by fertilization regimes (Liang et al., 2016). Nevertheless, a detailed chemical and size-related characterization of soil colloids and their depth distribution in rice paddies are scarce, even though such information is fundamental for further understanding their role in the biogeochemical cycling of elements in these agro-ecosystems.

Redox cycling can directly or indirectly favour the dispersion and stability of soil colloids due to (i) the reductive dissolution of Fe oxides under anoxic conditions, particularly of the most susceptible, SRO Fe phases that can serve as binding agents holding aluminosilicate particles together (Henderson et al., 2012; Ryan and Gschwend, 1992; Tadanier et al., 2005); (ii) the increase in the negative surface charge of colloids leading to interparticle electrostatic repulsion as a result of the shift in solution pH values above the point of zero charge (PZC) induced by Fe reduction (Buettner et al., 2014; Thompson et al., 2006); and (iii) the neoformation of colloidal Fe oxides and/or Fe-OM associations with a more negative surface charge (and lower PZC) due to higher OC surface loading during the oxidation of Fe(II) that often occurs in the presence of relatively high concentrations of DOC (i.e. coprecipitation; Sodano et al. 2017). These mechanisms are further confounded by the coupling effects of OM through direct association with colloids (Séquaris et al., 2013) or indirect influence on microbial Fe reduction via electron donation, electron shuttling and metal complexation (Royer et al., 2002). Moreover, OM can both favour colloid stability or destabilize them by causing the formation of aggregates as a function of OM concentration or composition (Yan et al., 2016).

The objectives of this work were to characterize the water-dispersible fine colloids (WDFC) in a temperate paddy soil and to provide insights into the influence of redox cycling on their depth distribution by comparison to an adjacent non-paddy soil. We hypothesized that (i) anaerobic conditions may lead to an overall increase in colloid concentration, and that (ii) colloidal mobility may represent an important C input to paddy subsoils. We therefore determined the amounts, size-distribution and chemical composition of WDFC isolated from soils collected from different horizons in adjacent arable plots under long-term paddy (P) and non-paddy (NP) management in NW Italy. Moreover, WDFC were also isolated from anaerobically-incubated topsoil samples to evaluate the changes in colloid distribution under reducing conditions as a function of management. Colloid characterization was carried out by asymmetric flow field-flow fractionation (AF4) coupled to different detectors in order to quantify OC, Fe, manganese (Mn), Al and Si in the different colloidal size fractions.

2. MATERIALS AND METHODS

2.1 Site description and sample collection

The study site is located in Zeme (Province of Pavia, NW Italy) (45°11'31.8"N; 8°40'3.7"E), in the plains of the River Po, between the Sesia and Agogna rivers. The study area has a temperate climate, with a mean annual temperature of 12.5°C and mean annual precipitation of 950 mm. Soils develop on alluvial sediment with a maximum elevation of 80 m a.s.l., characterized by a high groundwater level during spring, up to 30-50 cm below surface. Two adjacent plots were identified for this study, one under maize (*Zea mays*) monocropping (45°11'33.6"N 8°40'06.1"E; 1.35 ha) and another under paddy rice (*Oryza sativa*) monocropping established about 30 years ago (45°11'29.4"N, 8°40'04.5"E; 4.43 ha).

The maize crop was seeded in May and harvested in September with crop yields of about 16.5 t ha^{-1}. The rice crop was wet seeded (till 2008) or dry seeded (after 2008) in May, and harvested in October with crop yields of about 7.5-8 t ha^{-1}. Water management involved continuous flooding for most of the growing season, from just before seeding (wet seeded) or tillering (dry seeded) until ripening stages, except for one or two short (4 days) mid-season drainage periods for fertilizer and herbicide application. For both crops, fertilizer management during the cropping season followed conventional agronomical practices, while organic amendment (105-120 kg ha^{-1} horn and hoofs) and crop residues were incorporated with tillage (up to 25-30 cm) in autumn (November).

The soils forming under both cropping systems were clearly distinguishable and classified as Endogleyic Fluvisols under maize monocropping (NP, non-paddy) and Haplic Gleysols

under paddy management (P, paddy; IUSS World Reference Base, 2015). Basic properties of the soil horizons under non-paddy and paddy management are reported in Table 1. In the spring of 2018, soil samples were collected from each horizon from three replicated soil pits in each plot, air dried and homogenized to < 2 mm.

2.2 Quantification of pedogenetic oxides

Oxalate-extractable Fe, Mn and Al (Fe_o, Mn_o and Al_o, respectively) and dithionite-citrate-bicarbonate (DCB)-extractable Fe and Mn (Fe_d and Mn_d, respectively), were determined on soil samples as described by Schwertmann (1964) and Mehra and Jackson (1960). Metal concentration in the extracts were determined using atomic absorption spectroscopy (AAnalyst 400, Perkin Elmer). The ratio of the Fe_o/Fe_d, indicative of the contribution of the SRO phases to total pedogenetic oxides, as well as their difference to estimate the content of more crystalline oxides (Fe_c), were calculated.

2.3 Extraction of water-dispersible fine colloids

The water-dispersible colloids (WDC; < 20 μm) of 4 horizons from the non-paddy soil (Ap1, Ap2, Bgw and 3C) and 6 horizons from the paddy soil (Arp1, Arp2, Arpd, Brd1, Brd2 and 3C) were separated using the soil particle-size fractionation method of Séquaris and Lewandowski (2003). In brief, soil samples (6 g of dry soil basis) were suspended in ultrapure water (Milli-Q) in a soil:solution mass ratio of 1:2 and shaken for 6 hours. After the addition of 36 ml of ultrapure water to bring the soil:solution ratio to 1:8, suspensions were shaken by hand, and WDC suspensions were collected using a pipette after a 1.5 h sedimentation time determined according to Stokes' law. The WDC suspensions were subsequently centrifuged for 30 min at 1738 *g* and filtered through 0.45 μm membrane filters to obtain the suspension containing WDFC fraction < 450 nm.

Since the dispersion of soil colloids may be strongly influenced by short-term changes in soil redox potentials and pH caused by water saturation during flooding, WDFC were also separated from topsoil horizons (Ap1 and Ap2 from the non-paddy soil, and Arp1 and Arp2 from the paddy soil) incubated under anoxic conditions. Soil slurries made from 20 g of air dried soil aliquots suspended in 50 ml degassed, ultrapure water in crimp-top vials, were incubated anaerobically in the dark at 20 °C for 35 days after flushing the headspace with N_2. Over this incubation time pH increased to circum-neutral values, soil redox potentials decreased to +96 and +129 mV, and soil solution concentrations of Fe^{2+} and DOC increased to

values of 60 and 30 mg Fe l^{-1}, and 112 and 67 mg C l^{-1}, for the non-paddy and paddy soils, respectively (further details provided in 'Supplementary material').

After the incubation period, the suspensions were transferred into centrifugation tubes in a glove box with a N_2 atmosphere and diluted with 110 ml of degassed ultrapure water to obtain a soil:solution ratio of 1:8. The WDFC fractions were separated from the suspensions by sedimentation and centrifugation as described above, always maintaining anoxic conditions.

2.4 WDFC fractionation by asymmetric flow field-flow fractionation

Extracted WDFC were size-separated by asymmetric flow field-flow fractionation (AF4; AF2000, Postnova Analytics, Landsberg, Germany) with a 1 kDa polyethersulfone (PES) membrane, a 500 μm spacer and 25 μM NaCl solution as a carrier with a cross-flow of 2.5 ml min^{-1}. This technique provided a continuous separation of colloids and retention times were converted to hydrodynamic diameters by calibration with sulfate-stabilized polystyrene latex standard particles under the same analytical conditions as the samples (Jiang et al., 2015). The AF4 was coupled online to an organic C detector (OCD; DOC-Labor, Karlsruhe, Germany), and an inductively coupled plasma mass spectrometer (ICP-MS; Agilent 7500, Agilent Technologies, Japan) for monitoring Fe, Mn, Al and Si contents of the size-separated particles. Sample volumes of 50 and 200 μl were injected in the AF4-OCD and AF4-ICP-MS systems respectively, while a focusing time of 6 and 12 min were used, respectively. Further details of the AF4 technique and analytical element determination are described elsewhere (Jiang et al., 2015, 2017; Nischwitz et al., 2016). AF4 colloidal separation of anaerobically incubated samples was carried out as above but with a series of precautions to ensure oxygen-free conditions during sample analysis. These included sample handling under argon, the use of argon-purged carrier during both AF4 channel preparation and size-separation, as well as the flushing of solvent and syringe rinsing bottles with argon.

The OCD raw data were collected in volts of the detector signal (V) while the raw data of the ICP-MS measurements were collected in counts per second. After baseline correction, the peak areas of the separated particle fractions were integrated and converted to concentrations (mg l^{-1}) by means of linear, multipoint, flow injection calibration (Nischwitz et al., 2016). Total OC concentration in the WDFC was determined by elemental analysis and DOC (assumed to have a hydrodynamic diameter < 0.6 nm, the lower particle limit with a cut-off membrane of 1 kDa) was calculated as the difference between total OC and the sum of OC concentrations in the separated WDFC fractions.

3. RESULTS

3.1 Depth distribution of pedogenetic oxides

Pedogenetic Fe oxide contents (Fe_d) in the NP soils tended to decrease with depth, except for an increase in correspondence with the 2Bgw horizon at 65-80 cm (Table 2). Crystalline Fe oxides (Fe_c) mainly contributed to this increase in this horizon, as SRO Fe oxide contents (Fe_o) decreased steadily and the Fe_o/Fe_d ratio decreased from 0.49 to 0.21. In contrast, the distribution of pedogenetic Fe oxides with depth in the P soils showed very different trends. In particular, P topsoils were greatly depleted in both SRO and total Fe oxides with respect to NP soils, while subsoil horizons (Brd1, Brd2 and Bg1) has 2.6-3.7 times more Fe_o and 1.5-2.5 times more Fe_d with respect to the Bgw horizon corresponding to the same depth in NP (Table 2). Maximum Fe_c contents of 9.99 g kg^{-1} were also observed in correspondence with the Brd1 horizon (cf. 5.12 g kg^{-1} in the Bgw horizon of the NP soils). Along the whole profile, the pedogenetic Fe oxides in the P soils always showed a greater proportion of SRO Fe oxides (23 to 61%) with respect to the NP soils, particularly in the subsoil below the plough pan (Table 2).

Mean Mn_o and Mn_d values were relatively low in the NP soils with highest values in correspondence with the deepest horizons (2Bgw and 3C) and Mn_o/Mn_d values (> 0.73) increased slightly with soil depth (Table 2). In the P soils, Mn_o and Mn_d contents were barely detectable in the topsoil, while highest values of Mn_o and Mn_d were observed in the Brd2 subsoil horizon, with a Mn_o/Mn_d ratio of 0.84. Below this horizon, Mn_o and Mn_d values were similar or only slightly higher than those observed in the NP soils with similar Mn_o/Mn_d ratios (Table 2).

As for the SRO Fe oxides, Al_o tended to decrease with soil depth in the NP soils (Table 2). On the other hand, P topsoils were depleted in Al_o with respect to NP soils while all P subsoils showed significantly higher Al_o contents with respect to NP, with maximum concentrations in correspondence with the deep 2Cbw horizon (Table 2).

3.2 Colloidal organic C distribution in different size fractions

Total WDFC-associated OC decreased with depth from 7.01 to 0.52 mg C l^{-1} in the NP soils (Table 3). When compared to NP soils, P soils showed lower values in the A horizons but higher contents in correspondence with the Brd1 and Brd2 subsoil horizons where values as high as 9.43 mg C l^{-1} were observed (Table 3). AF4-OCD fractograms of WFDC extracted from the different topsoil and subsoil horizons of NP and P soils evidenced the presence of different-sized colloid fractions as a function of elution time (Fig. 1). After an initial small void

peak (1-2 min), three different colloid-sized fractions were defined based on the identification of three peak maxima in the WDFCs of most samples. The first distinct peak with a maximum around 13.5 min and a retention time between 13-25 min corresponded to a fraction with a particle size < 30 nm (F1). The peaks corresponding to the second and third size-fractions did not show baseline separation but often had clearly distinct peak maxima at around 39 and 47 min. We decided to integrate peak areas between 25 and 43 min, and between 43 and 70 min, corresponding to two particle-size colloid fractions of 30-240 nm (F2) and 240-450 nm (F3).

Fractograms evidenced important differences in the distribution of colloidal OC between horizons of the two soils (Fig. 1). Topsoil horizons had most OC associated with the F3 fraction (42-58% of total WDFC OC) under both management practices (Fig. 1a and b), with NP soils showing slightly higher absolute contents with respect to P soils (Table 3). In these horizons, about 31-54% of total WDFC OC was truly dissolved (i.e. < 0.6 nm defined as the lower particle cut-off for AF4 fractionation), with only minor proportions associated with the finer F1 and F2 fractions (3 and 5%, respectively).

The effect of anoxic conditions on the quantity and distribution of OC associated with fine colloids in the topsoils was strong. Anaerobic incubation increased total WDFC-associated OC by 2.7 and 3.4-fold for NP and P soils, respectively (Table 3). However, this increase was not consistent across fractions as F1, and to a lesser extent F2, showed the greatest increase both in absolute and relative terms (Fig. 1a and b; Table 3). Moreover, the observed increase in WDFC fractions under anoxic conditions was more consistent in P with respect to NP topsoils, even though absolute concentrations were either similar or slightly higher in the latter. In fact, anoxic conditions led to a 20.4 and 12.7-fold increase in the OC contents of the F1 and F2 fractions in P topsoils (up from < 3 % to ≈12 % of total WDFC-associated OC), while NP soils experienced only a 5.0 and 4.4-fold increase, respectively.

The lower contents of WDFC-associated OC in the B horizons of NP soils with respect to the oxic topsoils was consistent across fractions (Fig. 1c). In contrast, subsoil horizons in P soils showed particularly high OC contents associated with the F2 and F3 fractions, even higher with respect to OC contents of the same fractions in the topsoil, in both absolute and relative terms (Fig. 1d; Table 3). In fact, OC contents of the F2 fraction in Brd1 and Brd2 horizons were 11-22-fold higher with respect to the same fraction in the topsoil, and represented 16-24% of the total WDFC-associated OC. The F3 fraction in these horizons had an OC content that was only 3-fold higher with respect to the same fraction in the topsoil, but nonetheless represented the main constituent (57-62%) of the WDFC-associated OC (Fig. 1d; Table 3).

3.3 Elemental composition of water-dispersible fine colloids

Albeit with slightly different retention times due to differences in the focus times between the two analyses, AF4-ICP fractograms of the WFDC extracts evidenced similar colloid size-fractions as those observed by AF4-OCD, with the exception of F1 (< 30 nm) for which negligible amounts of all elements analyzed were detected and thus not quantifiable (Fig. 2). The mean total contents of Fe, Mn, Al and Si in WDFC extracted from the topsoil horizons (calculated as the sum of F2 and F3 fractions) were generally higher in NP with respect to P soils (~ 1.5 to 2.5-fold when quantifiable), and decreased in the order Si > Al > Fe > Mn (Fig. 2 a, b, e, f, i, j, o, p; Table 4). In most cases, element contents of the F3 fraction in all topsoils were only slightly higher than those of the F2 fraction (1.2 to 1.7-fold) irrespective of soil management. Calculated element molar ratios evidenced that both WDFC fractions had similar Fe/Al, Fe/Si and Si/Al ratios, although Fe/Al and Fe/Si ratios were slightly higher in NP with respect to P topsoils (Table 5). In contrast, the two WDFC fractions showed substantially different C/Fe molar ratios with higher values for the F3 with respect to the F2 fraction across both NP and P topsoils (Table 5).

Under anoxic conditions, the amounts of WDFC-associated Fe, Al and Si extracted from NP and P topsoils increased substantially compared to the same soils under oxic conditions (on average 4.4, 3.1 and 1.5-fold for Fe, Al and Si, respectively), while little changes in the contents of Mn were observed. However, in contrast to WDFC-associated OC, anoxic conditions did not alter the distribution of elements between different colloid size-fractions. In fact, similar increases were observed for the element contents of both F2 and F3 fractions (Table 4), and similar molar Fe/Al, Fe/Si and Si/Al ratios were observed for both fractions under anoxic conditions across soils (Table 5). When compared to oxic conditions, anoxia did however result in a slight increase in Fe/Al ratios, a strong increase in Fe/Si ratios, and a substantial decrease in Si/Al ratios of both WDFC fractions (Table 5). The different effects of anoxic conditions on the redox-driven changes in WDFC size-distribution of OC and Fe between NP and P soils resulted in differences in the variations in their C/Fe ratios too. In fact, whereas the C/Fe ratio of both F2 and F3 colloid fractions from the NP topsoils decreased after anoxic incubation, the C/Fe ratio of the F2 fraction in P topsoils increased while that of the F3 fraction decreased.

In NP subsoils, WDFC-associated Fe, Mn, Al and Si decreased drastically with soil depth (Fig. 2 c, g, k, o), except for the F3 fraction in the Bgw horizons that showed similar or only slightly lower contents than those found in the overlying A horizons (Table 4). C/Fe, Fe/Al and Fe/Si molar ratios also tended to decrease with soil depth, while Si/Al ratios of WDFC fractions remained relatively constant across the soil profile and within the range 2.14-2.42 (Table 5).

As for the depth distribution of WDFC-associated OC, fine colloids extracted from P subsoils showed significant enrichment in Fe, Mn, Al and Si in correspondence with the Brd1 and Brd2 horizons (Fig. 2 d, h, l, p; Table 4). In these horizons, the proportion of finer colloids in the F2 fraction was significantly higher than that in the F3 fraction, while the F1 fraction remained barely detectable. Moreover, the Brd1 horizons showed the highest contents of WDFC-associated Fe, Al and Si within the P profiles (Fig. 2 d, l, p), while colloidal Mn concentrations were highest in the Brd2 horizons (Fig 2. h). In the former horizons, Fe, Al and Si contents of the F2 fraction were 22, 10 and 9-fold higher with respect to the mean element contents of the corresponding WDFC fraction in the topsoils, respectively (Table 4). On the other hand, the F3 fractions were generally only between 3 to 7-fold higher. Nonetheless, Fe/Al, Fe/Si and Si/Al molar ratios of the two WDFC fractions in the Brd1 horizon were rather similar with values of about 0.46, 0.21 and 2.20, respectively. In contrast to NP soils, the Fe/Al and Fe/Si ratios of WDFC tended to increase with soil depth, C/Fe ratios decreased, while the Si/Al ratio only slightly decreased (Table 5).

4. DISCUSSION

4.1 Management induced changes on OC and Fe sesquioxide stocks

The larger accumulation of OM in soils under paddy management with respect to other arable ecosystems has been widely recognized to contribute to the C sink functions of rice agro-ecosystems (Kalbitz et al., 2013; Kögel-Knabner et al., 2010; Wissing et al., 2011). This has often been attributed to the retarded decomposition of OC under waterlogged conditions during several months of paddy field flooding every year (Sahrawat, 2004), although enhanced soil microaggregation (Wissing et al., 2014) and specific organo-mineral associations have also been shown to drive OC accrual in these redox-active soils (Winkler et al., 2019).

In this study, the soil under paddy management for over 30 years had topsoil OC stocks that were 55 % larger than that found in the adjacent non-paddy soil (Fig. 3). Our results are in accordance with the larger OC stocks in paddy soils compared to other agro-ecosystems reported for arable soils across Japan (Yagasaki and Shirato, 2014) and sub-tropical China (Wu, 2011). Moreover, the studied paddy soil also showed subsoil OC stocks (30-100 cm) that were 2.6-fold greater with respect to the non-paddy soil (Fig. 3). Various studies suggest that the lower microbial activity and increased association with mineral surfaces in the subsoil lead to the longer turnover times of deep OC with respect to surface soil OC (Harrison et al., 2011; Kramer et al., 2012). Consequently, similar mechanisms in paddy subsoils may potentially contribute to the long-term deep soil OC accumulation in these temperate agro-ecosystems.

However, this would directly depend on the input of OC into the subsoil as well as pedogenetic processes driving the evolution of mineral surfaces in the subsoil. Previous studies carried out on subtropical paddy soil chronosequences developing on marine sediments have evidenced that OC accrual in topsoils under long-term paddy management may not always correspond to an increase in OC stocks in the subsoil (Kalbitz et al., 2013; Wissing et al., 2011). This has been attributed to the low permeability of the dense plough pan that may act as a transport barrier limiting OC entry into subsoil horizons. Nevertheless, Said-Pullicino et al. (2016) reported that DOC (< 0.45 μm) fluxes from the topsoil to the subsoil in relatively young, temperate rice paddies developing on alluvial deposits and managed under continuous flooding, may be as high as 33–51 g C m^{-2} yr^{-1}, contributing substantially to OC inputs into the deeper soil horizons.

The interaction of OC with soil minerals and its subsequent stabilization against microbial mineralization (Eusterhues et al., 2014) could largely depend on soil redox conditions. Apart from affecting OC stocks, paddy management caused notable differences in the amounts, depth distribution and crystallinity of Fe oxides along the soil profile with respect to the non-paddy soil. The slightly higher total Fe sesquioxide stocks in the paddy with respect to the non-paddy soil (14.1 and 11.8 kg m^{-2} up to 1 m, respectively) suggest that lateral transport of dissolved and/or colloidal Fe under paddy management was not relevant in this poorly developed, coarse-textured soil, as opposed to the significant loss of Fe through this pathway considered to be responsible for the loss in Fe stocks in paddy soils with a fine-textured low permeability plough pan (Winkler et al. 2016).

Paddy topsoil horizons were depleted in both SRO and crystalline Fe oxides (Table 2) and consequently pedogenetic Fe oxide stocks were 33 % lower with respect to the non-paddy soil (Fig. 3) even though paddy topsoils still showed a greater proportion of Fe_o (Table 2). On the other hand, paddy subsoil horizons just beneath the plough pan (Brd1) were enriched in Fe oxides, particularly SRO oxides (Table 2). This accounted for a 43 % increase in subsoil Fe oxide stocks with respect to the adjacent non-paddy soil (Fig. 3). Similar trends were observed for oxalate-extractable Mn and Al, although accumulation in the subsoil occurred in deeper horizons, namely Brd2 and 2Cbw, respectively. Anoxic conditions in the plough layer of paddy soils during the cropping season causes the reductive dissolution of Fe oxides leading to an increase in porewater Fe(II) concentrations, particularly in the presence of freshly incorporated crop residues (Bertora et al., 2018; Said-Pullicino et al., 2016). Subsequent oxidative precipitation of dissolved Fe(II) can occur either in the topsoil with the re-establishment of oxic conditions or in the O_2-rich rice rhizosphere, or in the more oxic subsoil following leaching

through the plough pan. This leads to the formation of new mineral phases, mainly SRO oxides more or less associated with phyllosilicate particles (Kirk, 2004; Sodano et al., 2016) or Fe-OC coprecipitates (Sodano et al., 2017) which can contribute to the retention of OC.

Various studies have evidenced that soils experiencing dynamic redox conditions due to intense rainfall or paddy management generally show a decrease in total amounts of Fe oxides in the topsoil with an increase in the proportion of SRO Fe oxides (Thompson et al., 2011; Kölbl et al. 2014). The consequent distribution of Fe oxides along the soil profile were suggested to depend on the texture-related permeability of the soil and its effect on the balance between Fe oxide dissolution in the topsoil and Fe(II) leaching rates into the subsoil or lateral transport (Kölbl et al. 2014; Winkler et al., 2016). Considering the coarse-texture of the paddy soil studied in this work, leaching rates were probably faster than the dissolution of the more crystalline Fe phases contributing to the depletion of SRO minerals in paddy with respect to non-paddy topsoils. Based on the data provided in Said-Pullicino et al. (2016) and following the same methodology applied for DOC, we estimated Fe(II) fluxes from the topsoil into the subsoil by multiplying daily extrapolated porewater Fe(II) concentrations at a depth of 25 cm by the water percolation fluxes over the cropping season. The obtained fluxes in the order 25-42 g m^{-2} yr^{-1}, are commensurate with the observed decrease in topsoil Fe oxide stocks under paddy management (Fig. 3). We therefore postulate that the higher proportion of SRO minerals observed after 30 years of different soil management provided a higher potential for OC accumulation in these paddy soils compared to soils developing on the same parent material but under non-paddy management, especially in the subsoil.

4.2 Redox-induced changes of water-dispersible fine colloids in the topsoil

Most evaluations of DOC and Fe mobility in rice paddies have been made on soil solutions passed through 0.45-µm membrane filters, disregarding the presence of nanoparticles (Said-Pullicino et al., 2016; Xu et al., 2013). However, various studies have found that colloids < 450 nm easily dispersed from soil and with different OM and elemental composition, can contribute significantly to element mobility in a range of redoximorphic soils (Henderson et al., 2012; Jiang et al., 2015).

The fractograms of the WDFC extracted from paddy and non-paddy soils evidenced a size-resolved separation of nanoparticles < 30 nm and two fine colloidal fractions (30-240 nm and > 240 nm). The < 30 nm size-fraction mainly contained OM, as it was difficult to identify the presence of Fe, Al and Si due to their low concentrations. The fine colloidal fractions 30-240 nm and > 240 nm had relatively similar Al and Fe contents and an Si/Al molar ratio ≈ 2 (Table

5), indicative of the presence of Fe and Al (hydr)oxides associated with 2:1 type phyllosilicate minerals (Figs. 1 and 2). Similar size distributions and compositions were observed for water-dispersible colloids separated from arable soils (Jiang et al., 2015).

Colloidal organic C in both paddy and non-paddy soils was mainly associated with the largest WDFC size fraction (i.e. > 240 nm), and the co-elution of substantial amounts of Fe and the highest C/Fe molar ratio measured for this fraction (Tables 4 and 5), likely indicate the presence of Fe (hydr)oxides known to have a strong affinity for DOC (Mikutta et al., 2006) and an important role in binding of particles in fine colloidal aggregates (Henderson et al., 2012; Jiang et al., 2015). Similarly, Sodano et al. (2017) showed that coprecipitation of Fe and OC during the oxidation and hydrolysis of Fe^{2+}, can lead to a high retention of C within highly aggregated Fe-OM associations. Finally, a considerable proportion of extracted OC (around 43%) was truly dissolved (< 1 kDa).

Incubation of the topsoils under anoxic conditions increased colloidal dispersion across size-fractions with a preferential release of OC associated with the nano-sized (< 30 nm) and small-sized (30-240 nm) colloidal particles for both soils (Fig. 1). Various studies on redoximorphic soils have evidenced an increase in DOC concentrations (< 450 nm) under reducing conditions in both laboratory microcosms (Dunham-Cheatham et al., 2020; Grybos et al., 2009; Hanke et al., 2013; Winkler et al. 2019) and in the field (Bertora et al., 2018; Said-Pullicino et al., 2016) partly due to OC release as a result of the reductive dissolution of Fe oxides and the increase in soil pH under anaerobic conditions. However, these studies did not distinguish between truly dissolved and colloidal OC pools. Our results suggest that colloidal C is an important contributor to mobile OC, and only a limited portion of OC released under anoxic conditions is truly dissolved (20-40%).

The reductive dissolution of Fe oxides in C-rich aggregate particles and the consequent shift in pH to values higher than the PZC of colloidal particles (Thompson et al., 2006) were probably responsible for the increase in Fe, Al and Si contents of the > 30 nm colloidal fractions (Fig. 2). This is in line with the findings of Buettner et al. (2014) who show that Fe reduction was mainly responsible for the dispersion of larger colloids, while increasing pH dispersed primarily the smallest colloids under anoxic conditions. Moreover, the decrease in the colloidal Si/Al molar ratio under reducing conditions (Table 5) suggests that a substantial amount of mobilized Al probably derived from the release of Al–organic complexes associated with readily reducible SRO Fe oxide minerals, known to be present in the rice rhizosphere (Kölbl et al., 2017), rather than exclusively from the dispersion of 2:1 type phyllosilicates.

Repeated management-induced redox cycling was probably responsible for an enhanced colloidal dispersion and mobilization leading to the depletion of OC-containing WDFC (Table 3), and substantially lower colloidal Fe, Al and Si (as well as lower Fe/Al and Fe/Si ratios) observed in the paddy with respect to the non-paddy topsoils (Table 4). Thompson et al. (2006) showed an increase in colloid stability with repeated Fe reduction and oxidation cycles involving a redoximorphic tropical topsoil. Similarly, Jiang et al. (2017) also evidenced increasing concentrations of OC, Fe and Al in nano-sized and small-sized colloids in three grasslands sites with increasing influence of stagnic conditions.

Although topsoils under long-term paddy management were depleted in WDFC with respect to non-paddy soils, the relative increase in the dispersion of OC associated with the finest colloids (< 30 and 30-240 nm) under reducing conditions was nonetheless greater in the paddy soil (Fig. 1). This seems to suggest that redox cycling continuously replenished the formation of finer colloidal material readily dispersed with the establishment of anaerobic conditions. This is corroborated by previous findings that showed that Fe (hydr)oxides formed during the oxidation of Fe^{2+} in solution are composed of nanometric particles, more or less aggregated as a function of the concentrations of DOC in solution during coprecipitation (Pédrot et al., 2011; Sodano et al., 2017).

4.3 Redox-induced changes of water-dispersible fine colloids in the subsoil

The downward mobilization of colloidal organo-mineral associations can represent an important process driving OC stabilization in paddy subsoils, contributing to the long-term accumulation of OC in these agro-ecosystems. Our results clearly evidence that long-term paddy management led to a significantly greater amount of WDFC in correspondence with the illuvial Brd horizons just beneath the plough pan, with respect to non-paddy subsoils (Fig. 1 and 2). This is in line with the higher contents of total OC and pedogenetic (hydr)oxides in paddy with respect to non-paddy subsoils (Tables 1 and 2), that suggest that redox-driven processes may control OC and Fe input to the subsoil. Liang et al. (2016) also reported an increase in the mass of soil colloidal particles with soil depth in a long-term subtropical fine-textured paddy soil.

The observed increase in fine colloids (Tables 3 and 4) and Fe^{2+} (Fig. S1c) in the topsoil under anaerobic conditions, together with the relatively high percolation water fluxes could have been responsible for the transport of colloidal particles and dissolved Fe^{2+} in soil matrix and preferential flow during rice cropping. On one hand, organic C and Fe oxide-rich aluminosilicate particles (C/Fe ≈ 1 and Fe/Si ≈ 0.3) with a high colloidal stability (Thompson

et al., 2006) released from the topsoil under anoxic conditions and mobilized along the soil profile could have been partly responsible for the accumulation of WDFC in the paddy subsoil horizons (Fig. 1 and 2), as well as for the finer soil texture and higher bulk density (i.e. lower porosity) of the illuvial Brd horizons having a clay content that was double that in the topsoil under paddy management (Table 1). Moreover, the greater Fe, Al and Si contents in the finer (30-240 nm) than the coarser (> 240 nm) WDFC fraction in the Brd horizons (Fig. 2 l and p; Table 4) nearly an order of magnitude higher with respect to the topsoil horizons, are in line with a greater mobility of smaller-sized particles through the preferential flow pathways that transport water through the dense plough pan.

On the other hand, the percolation of Fe^{2+} (and Mn^{2+}) released into solution during the reductive dissolution of metal oxides in the topsoil under anoxic conditions (Fig. S1c), towards the more oxic subsoil could have led to the *in situ* formation of fine colloids beneath the plough pan as a result of the (co-)precipitation of SRO oxides (together with DOC). Colloidal Fe and Mn in the Brd horizons were more abundant with respect to the topsoil (13-fold for total colloidal Fe), and mainly associated with the finer (30-240 nm) and, to a lesser extent, the coarser-sized (> 240 nm) WDFC fractions. Although oxidation of Fe^{2+} solutions was shown to result in the formation of nanoparticles (Pédrot et al., 2011; Sodano et al., 2017), in the presence of negatively charged 2:1 type phyllosilicates, clay mineral surfaces can govern the precipitation of Fe leading to the formation of non-homogeneous Fe (hydr)oxide coatings (Sodano et al., 2016). Moreover, when Fe(II) is re-oxidized in the presence of high DOC concentrations or in horizons with high OM contents, the resulting Fe(III) phases are likely to have a low crystalline order and be less susceptible to ripening to more crystalline phases via Fe(II) catalyzed atom exchange processes (Chen et al., 2018; Chen and Thompson, 2018; Jones et al., 2009). Further support for the *in situ* process of subsoil colloid formation is provided by the higher concentrations of colloidal Mn determined in the deeper Brd2 horizon with respect to Brd1 horizon where colloidal Fe is most abundant. This could be directly attributed to the higher reduction potential of Mn(IV) with respect to Fe(III) (Kirk, 2004), that would explain the mobilization of dissolved Mn^{2+} through the plough pan and subsequent precipitation in correspondence with deeper oxic horizons with respect to Fe^{2+}. These findings are in line with the field observation of pedogenetic features namely abundant mottling and common concretions in correspondence with the Brd1 and Brd2 horizons indicating the localized precipitation of Fe and Mn SRO phases.

The processes leading to the higher amounts of colloidal OC in the paddy subsoil with respect to the non-paddy soil could be various, although all indicate a redox-driven increase in

OC mobility along the soil profile. The mobilization of OC to deep mineral horizons in redoximorphic soils due to Fe oxide reduction and subsequent release of OM into the colloidal phase has been reported for basaltic soils under tropical forest in Hawaii (Buettner et al., 2014). The preferential release of nanoparticles and fine colloids observed in anoxic paddy topsoils (Fig. 1b), was however not reflected in a similar distribution in the subsoil horizons (Fig. 1 d) where most OC was associated with the larger size-fraction (≈ 60% of OC in WDFC) and less than 2 % of OC in WDFC was associated with the < 30 nm fraction (Table 3). The organic nanoparticles released under anoxic conditions were probably preferentially retained by adsorption or coprecipitation in the topsoil and/or during passage through the plough pan. Moreover, DOC and fine colloidal material reaching the subsoil could have also led to substantial particle aggregation in these deeper soil horizons, rich in pedogenetic SRO oxides. On the other hand, the relatively high C/Fe ratio of the larger colloidal fraction in the topsoil indicated substantial OM coatings on the mineral colloids, imparting a more negative surface charge at near neutral pH (Buettner et al., 2014). This was probably responsible for their high colloidal stability and greater contribution OC migration to the deeper illuvial horizons.

5. CONCLUSIONS

Our findings confirm our hypothesis that anaerobic conditions enhance colloidal dispersion, with a tendency to favour the release/formation of finer particle fractions. Long-term rice cultivation eventually results in a depletion of colloidal material in the oxic topsoil indicating that the particular hydrology of these relatively coarse-textured paddy soils can lead to a substantial colloidal mobility along the soil profile. Nevertheless, these temperate paddy soils still showed substantial dispersion of the finest colloids under reducing conditions, suggesting that long-term redox cycling does not only favour colloid dispersion and mobilization, but also influences their size distribution.

The transport of organo-mineral colloids, together with truly dissolved OC, represents an important input of OC into deeper soil horizons with percolating water. This colloid transport, together with the percolation of Fe^{2+} and subsequent precipitation in the oxic subsoil horizons, could have contributed to the observed accumulation of colloidal material in the illuvial horizons, as well as the higher OC and SRO Fe oxide stocks in temperate paddy with respect to non-paddy subsoils.

Acknowledgements

This study was funded by the University of Torino as part of the research project "Colloid

mobility and organic matter stabilization in hydromorphic soils". We also like to express our gratitude to Cristina Lerda for her assistance with the analysis.

References

Bertora, C., Cucu, M.A., Lerda, C., Peyron, M., Bardi, L., Gorra, R., Sacco, D., Celi, L., Said-Pullicino, D., 2018. Dissolved organic carbon cycling, methane emissions and related microbial populations in temperate rice paddies with contrasting straw and water management. Agric Ecosyst Environ 265, 292-306.

Buettner, S.W., Kramer, M.G., Chadwick, O.A., Thompson, A., 2014. Mobilization of colloidal carbon during iron reduction in basaltic soils. Geoderma 221-222, 139-145.

Chen, C., Meile, C., Wilmoth, J., Barcellos, D., Thompson, A., 2018. Influence of pO_2 on iron redox cycling and anaerobic organic carbon mineralization in a humid tropical forest soil. Environ Sci Technol 52, 7709-7719.

Chen, C., Thompson, A., 2018. Ferrous iron oxidation under varying pO_2 levels: The effect of Fe(III)/Al(III) oxide minerals and organic matter. Environ Sci Technol 52, 597-606.

Cheng, Y.Q., Yang, L.Z., Cao, Z.H., Ci, E., Yin, S., 2009. Chronosequential changes of selected pedogenic properties in paddy soils as compared with non-paddy soils. Geoderma 151, 31-41.

Chorover, J., Amistadi, M.K., Chadwick, O.A., 2004. Surface charge evolution of mineral-organic complexes during pedogenesis in Hawaiian basalt. Geochim Cosmochim Acta 68, 4859-4876.

Dunham-Cheatham, S.M., Zhao, Q., Obrist, D., Yang, Y., 2020. Unexpected mechanism for glucose-primed soil organic carbon mineralization under an anaerobic-aerobic transition. Geoderma 376, 114535.

Eusterhues, K., Neidhardt, J., Hädrich, A., Küsel, K., Totsche, K.U., 2014. Biodegradation of ferrihydrite-associated organic matter. Biogeochemistry 119, 45-50.

Grybos, M., Davranche, M., Gruau, G., Petitjean, P., Pédrot, M., 2009. Increasing pH drives organic matter solubilization from wetland soils under reducing conditions. Geoderma 154, 13-19.

Hall, S.J., Berhe, A.A., Thompson, A., 2018. Order from disorder: do soil organic matter composition and turnover co-vary with iron phase crystallinity? Biogeochemistry 140, 93-110.

Hanke, A., Cerli, C., Muhr, J., Borken, W., Kalbitz, K., 2013. Redox control on carbon mineralization and dissolved organic matter along a chronosequence of paddy soils. Eur J

Soil Sci 64, 476-487.

Harrison, R.B., Footen, P.W., Strahm, B.D., 2011. Deep soil horizons: contribution and importance to soil carbon pools and in assessing whole-ecosystem response to management and global change. For Sci 57, 67-76.

Henderson, R., Kabengi, N., Mantripragada, N., Cabrera, M., Hassan, S., Thompson, A., 2012. Anoxia-induced release of colloid- and nanoparticle-bound phosphorus in grassland soils. Environ Sci Technol 46, 11727-11734.

Huang, W., Hall, S.J., 2017. Elevated moisture stimulates carbon loss from mineral soils by releasing protected organic matter. Nature Comm 8, 1774.

Huang, X., Kang, W., Guo, J., Wang, L., Tang, H., Li, T., Yu, G., Ran, W., Hong, J., Shen, Q., 2020. Highly reactive nanomineral assembly in soil colloids: Implications for paddy soil carbon storage. Sci Total Environ 703, 134728.

IUSS Working Group WRB, 2015. World Reference Base for Soil Resources 2014, update 2015: International soil classification system for naming soils and creating legends for soil maps. World Soil Resources Reports No. 106. FAO, Rome.

Jiang, X., Bol, R., Nischwitz, V., Siebers, N., Willbold, S., Vereecken, H., Amelung, W., Klumpp, E., 2015. Phosphorus containing water dispersible nanoparticles in arable soil. J Environ Qual 44, 1772-1781.

Jiang, X., Bol, R., Cade-Menun, B.J., Nischwitz, V., Willbold, S., Bauke, S., Vereecken, H., Amelung, W., Klumpp, E., 2017. Colloid-bound and dissolved phosphorus species in topsoil water extracts along a grassland transect from Cambisol to Stagnosol. Biogeosciences 14, 1153-1164.

Jones, A.M., Collins, R.N., Rose, J., Waite, T.D., 2009. The effect of silica and natural organic matter on the Fe(II)-catalysed transformation and reactivity of Fe(III) minerals. Geochim Cosmochim Acta 73, 4409-4422.

Kalbitz, K., Kaiser, K., Fiedler, S., Kölbl, A., Amelung, W., Bräuer, T., Cao, Z., Don, A., Grootes, P., Jahn, R., Schwark, L., Vogelsang, V., Wissing, L., Kögel-Knabner, I., 2013. The carbon count of 2000 years of rice cultivation. Glob Chang Biol 19, 1107-1113.

Katoh, M., Murase, J., Hayashi, M., Matsuya, K., Kimura, M., 2004. Nutrient leaching from the plow layer by water percolation and accumulation in the subsoil in an irrigated paddy field. Soil Sci Plant Nutr 50, 721-729.

King, E.K., Thompson, A., Pett-Ridge, J.C., 2019. Underlying lithology controls trace metal mobilization during redox fluctuations. Science of the Total Environment 665, 1147-1157.

Kirk, G. 2004. The Biogeochemistry of Submerged Soils. John Wiley & Sons, Chichester, U.K.

291 pp. ISBN 0-470-86301-3.

Kögel-Knabner, I., Amelung, W., Cao, Z., Fiedler, S., Frenzel, P., Jahn, R., Kalbitz, K., Kölbl, A., Schloter, M., 2010. Biogeochemistry of paddy soils. Geoderma 157, 1–14.

Kölbl, A., Schad, P., Jahn, R., Amelung, W., Bannert, A., Cao, Z.H., Fiedler, S., Kalbitz, K., Lehndorff, E., Müller-Niggemann, C., Schloter, M., Schwark, L., Vogelsang, V., Wissing, L., Kögel-Knabner, I., 2014. Accelerated soil formation due to paddy management on marshlands (Zhejiang Province, China). Geoderma 228–229, 67-89.

Kölbl, A., Schweizer, S.A., Mueller, C., Höschen, C., Said-Pullicino, D., Romani, M., Lugmeier, J., Schlüter, S., Kögel-Knabner, I., 2017. Legacy of rice roots as encoded in distinctive microsites of oxides, silicates, and organic matter. Soils 2017, 1(1), 2.

Kramer, M.G., Sanderman, J., Chadwick, O.A., Chorover, J., Vitousek, P.M., 2012. Long-term carbon storage through retention of dissolved aromatic acids by reactive particles in soil. Glob Chang Biol 18, 2594-2605.

Lalonde, K., Mucci, A., Ouellet, A., Gélinas, Y., 2012. Preservation of organic matter in sediments promoted by iron. Nature 483, 198-200.

Liang, X., Jin, Y., Zhao, Y., Wang, Z., Yin, R., Tian, G., 2016. Release and migration of colloidal phosphorus from a typical agricultural field under long-term phosphorus fertilization in southeastern China. J Soil Sediment 16, 842-853.

Marin-Spiotta, E., Chadwick, O.A., Kramer, M., Carbone, M.S., 2011. Carbon delivery to deep mineral horizons in Hawaiian rain forest soils. Journal of Geophysical Research: Biogeosciences 116, G03011.

Mehra, O.P., Jackson, M.L., 1960. Iron oxide removal from soils and clays by dithionite–citrate systems buffered with sodium bicarbonate. Clay Clay Miner 7, 317-327.

Mikutta, R., Kleber, M., Torn, M.S., Jahn, R., 2006. Stabilization of soil organic matter: Association with minerals or chemical recalcitrance? Biogeochemistry 77, 25-56.

Mikutta, R., Schaumann, G.E., Gildemeister, D., Bonneville, S., Kramer, M.G., Chorover, J., Chadwick, O.A., Guggenberger, G., 2009. Biogeochemistry of mineral-organic associations across a long-term mineralogical soil gradient (0.3-4100 kyr), Hawaiian Islands. Geochim Cosmochim Acta 73, 2034-2060.

Mikutta, R., Lorenz, D., Guggenberger, G., Haumaier, L., Freund, A., 2014. Properties and reactivity of Fe-organic matter associations formed by coprecipitation versus adsorption: clues from arsenate batch adsorption. Geochim Cosmochim Acta 144, 258-276.

Missong, A., Bol, R., Nischwitz, V., Krüger, J., Lang, F., Siemens, J., Klumpp, E., 2018. Phosphorus in water dispersible-colloids of forest soil profiles. Plant Soil 427, 71-86.

Nischwitz, V., Gottselig, N., Missong, A., Meyn, T., Klumpp, E., 2016. Field flow fractionation online with ICP-MS as novel approach for the quantification of fine particulate carbon in stream water samples and soil extracts. J Anal At Spectrom 31, 1858-1868.

Pédrot, M., Boudec, A. Le, Davranche, M., Dia, A., Henin, O., 2011. How does organic matter constrain the nature, size and availability of Fe nanoparticles for biological reduction? J Colloid Interface Sci 359, 75-85.

Roth, P.J., Lehndorff, E., Cao, Z. h., Zhuang, S., Bannert, A., Wissing, L., Schloter, M., Kögel-Knabner, I., Amelung, W., 2011. Accumulation of nitrogen and microbial residues during 2000 years of rice paddy and non-paddy soil development in the Yangtze River Delta, China. Glob Chang Biol 17, 3405-3417.

Royer, R.A., Burgos, W.D., Fisher, A.S., Unz, R.F., Dempsey, B.A., 2002. Enhancement of biological reduction of hematite by electron shuttling and Fe(II) complexation. Environ Sci Technol 36, 1939-1946.

Rumpel, C., Kögel-Knabner, I., 2011. Deep soil organic matter-a key but poorly understood component of terrestrial C cycle. Plant Soil 338, 143-158.

Ryan, J.N., Gschwend, P.M., 1992. Effect of iron diagenesis on the transport of colloidal clay in an unconfined sand aquifer. Geochimica et Cosmochimica Acta 56, 1507-1521.

Sahrawat, K.L., 2004. Organic matter accumulation in submerged soils. Adv Agron 81, 169-201.

Said-Pullicino, D., Miniotti, E.F., Sodano, M., Bertora, C., Lerda, C., Chiaradia, E.A., Romani, M., Cesari de Maria, S., Sacco, D., Celi, L., 2016. Linking dissolved organic carbon cycling to organic carbon fluxes in rice paddies under different water management practices. Plant Soil 401, 273-290.

Scharlemann, J.P.W., Tanner, E.V.J., Hiederer, R., Kapos, V., 2014. Global soil carbon: Understanding and managing the largest terrestrial carbon pool. Carbon Manag 5, 81-91.

Schwertmann, U., 1964. Differenzierung der Eisenoxide des Bodens durch Extraktion mit saurer Ammonium-oxalat Lösung. Z Pflanzenernaehr Dueng Bodenkd 105, 194-202.

Séquaris, J.M., Lewandowski, H., 2003. Physicochemical characterization of potential colloids from agricultural topsoils. Colloid Surf A: Physicochem Eng Asp 217, 93-99.

Séquaris, J.M., Klumpp, E., Vereecken, H., 2013. Colloidal properties and potential release of water-dispersible colloids in an agricultural soil depth profile. Geoderma 193–194, 94-101.

Sodano, M., Said-Pullicino, D., Fiori, A.F., Catoni, M., Martin, M., Celi, L., 2016. Sorption of paddy soil-derived dissolved organic matter on hydrous iron oxide-vermiculite mineral

phases. Geoderma 261, 169-177.

Sodano, M., Lerda, C., Nisticò, R., Martin, M., Magnacca, G., Celi, L., Said-Pullicino, D., 2017. Dissolved organic carbon retention by coprecipitation during the oxidation of ferrous iron. Geoderma 307, 19-29.

Tadanier, C.J., Schreiber, M.E., Roller, J.W., 2005. Arsenic mobilization through microbially mediated deflocculation of ferrihydrite. Environ Sci Technol 39, 3061-3068.

Thompson, A., Chadwick, O.A., Boman, S., Chorover, J., 2006. Colloid mobilization during soil iron redox oscillations. Environ Sci Technol 40, 5743-5749.

Thompson, A., Rancourt, D.G., Chadwick, O.A., Chorover, J., 2011. Iron solid-phase differentiation along a redox gradient in basaltic soils. Geochim Cosmochim Acta 75, 119-133.

Wang, L., Missong, A., Amelung, W., Willbold, S., Prietzel, J., Klumpp, E., 2020. Dissolved and colloidal phosphorus affects P cycling in calcareous forest soils, Geoderma, 375, 114507.

Winkler, P., Kaiser, K., Kölbl, A., Kühn, T., Schad, P., Urbanski, L., Fiedler, S., Lehndorff, E., Kalbitz, K., Utami, S.R., Cao, Z., Zhang, G., Jahn, R., Kögel-Knabner, I., 2016. Response of Vertisols, Andosols, and Alisols to paddy management. Geoderma 261, 23-35.

Winkler, P., Kaiser, K., Jahn, R., Mikutta, R., Fiedler, S., Cerli, C., Kölbl, A., Schulz, S., Jankowska, M., Schloter, M., Müller-Niggemann, C., Schwark, L., Woche, S.K., Kümmel, S., Utami, S.R., Kalbitz, K., 2019. Tracing organic carbon and microbial community structure in mineralogically different soils exposed to redox fluctuations. Biogeochemistry 143, 31-54.

Wissing, L., Kölbl, A., Vogelsang, V., Fu, J.R., Cao, Z.H., Kögel-Knabner, I., 2011. Organic carbon accumulation in a 2000-year chronosequence of paddy soil evolution. Catena 87, 376-385.

Wissing, L., Kölbl, A., Schad, P., Bräuer, T., Cao, Z.H., Kögel-Knabner, I., 2014. Organic carbon accumulation on soil mineral surfaces in paddy soils derived from tidal wetlands. Geoderma 228–229, 90-103.

Wu, J., 2011. Carbon accumulation in paddy ecosystems in subtropical China: evidence from landscape studies. Eur J Soil Sci 62, 29-34.

Yagasaki, Y., Shirato, Y., 2014. Assessment on the rates and potentials of soil organic carbon sequestration in agricultural lands in Japan using a process-based model and spatially explicit land-use change inventories – Part 1: Historical trend and validation based on nation-wide soil monitoring. Biogeosciences 11:4429-42.

Yan, J., Lazouskaya, V., Jin, Y., 2016. Soil colloid release affected by dissolved organic matter and redox conditions. Vadose Zone J 15, vzj2015.2002.0026.

715

Figure captions

Fig. 1. Asymmetric flow field-flow fractionation (AF4) organic C fractograms of water-dispersable fine colloids (WDFC) extracted from superficial (a, b) and sub-superficial (c, d) horizons under non-paddy (a, c) and paddy (b, c) management. Dashed lines in (a) and (b) represent the organic C fractograms of WDFC extracted from superficial soil samples after in vitro incubation under anoxic conditions.

Fig. 2. Asymmetric flow field-flow fractionation (AF4) fractograms of water-dispersable fine colloids (WDFC) extracted from superficial (a, b, e, f, i, j, o, p) and sub-superficial (c, d, g, h, k, l, o, p) horizons under non-paddy (a, c, e, g, i, k, m, o) and paddy (b, d, f, h, j, l, n, p) management, showing Al, Si, Fe and Mn mass flow monitored by inductively coupled plasma mass spectrometry. "Anoxic"-labelled series in superficial horizons (a, b, e, f, i, j, o, p) represent the fractograms of WDFC extracted from superficial soil samples after in vitro incubation under anoxic conditions.

Fig. 3. Organic C (a), and short-range ordered (Fe_o) and crystalline (Fe_c) Fe oxide (b) stocks in topsoil (0-30 cm) and subsoil (30-100 cm) horizons under non-paddy (NP) and paddy (P) management. Error bars represent standard error.

Table 1. Basic properties of the soil horizons from three replicated soil pits under non-paddy and paddy management.

Soil/Horizon	Depth (cm)	Sand (g kg^{-1})	Silt (g kg^{-1})	Clay (g kg^{-1})	Texture class[a]	Bulk density (g cm^{-3})	$pH_{(H2O)}$	OC[b] (g kg^{-1})	N_t[c] (g kg^{-1})	OC/N_t
Non-paddy										
Ap1	0-15	749	202	48	LS	1.59 ± 0.02	5.4 ± 0.1	7.79 ± 0.19	0.60 ± 0.01	13.0
Ap2	15-30	743	201	56	SL	1.43 ± 0.03	5.4 ± 0.1	7.95 ± 0.24	0.70 ± 0.02	11.4
Bgw	30-65/70	892	83	25	S	1.68 ± 0.04	5.7 ± 0.1	1.30 ± 0.06	0.09 ± 0.00	14.0
2Bgw	65-80	970	15	15	S	1.54 ± 0.09	5.9 ± 0.1	0.59 ± 0.04	0.05 ± 0.00	12.4
3C	80-100+	971	16	13	S	1.49 ± 0.01	6.0 ± 0.2	0.29 ± 0.16	0.02 ± 0.01	12.0
Paddy										
Arp1	0-13	709	237	53	SL	1.58 ± 0.02	5.7 ± 0.1	10.31 ± 0.39	0.81 ± 0.04	12.8
Arp2	13-25	714	243	43	SL	1.65 ± 0.08	5.6 ± 0.0	11.29 ± 0.51	0.92 ± 0.01	12.3
Arpd	25-34	683	253	63	SL	1.79 ± 0.06	5.6 ± 0.1	7.19 ± 1.20	0.59 ± 0.11	12.2
Brd1	34-43	702	188	109	SL	2.01 ± 0.08	6.6 ± 0.1	3.20 ± 0.22	0.24 ± 0.01	13.5
Brd2	43-53	742	149	109	SL	1.98 ± 0.05	6.6 ± 0.1	2.57 ± 0.07	0.22 ± 0.00	11.7
Bg1	53-68	753	141	106	SL	1.68 ± 0.02	6.5 ± 0.1	2.50 ± 0.19	0.21 ± 0.01	12.0
Bg2	68-80	861	70	70	LS	1.55 ± 0.02	6.5 ± 0.1	1.98 ± 0.09	0.17 ± 0.00	11.6
2CBw	80-100	946	26	29	S	1.73 ± 0.03	6.6 ± 0.1	1.38 ± 0.14	0.10 ± 0.01	13.5
3C	100+	972	15	13	S	1.51 ± 0.02	6.8 ± 0.1	0.64 ± 0.05	0.05 ± 0.01	12.6

[a] Texture: SL, sandy loam; LS, loamy sand; S, sand.
[b] Organic carbon
[c] Total nitrogen

Table 2. Pedogenetic Fe, Mn and Al oxides contents with depth in soils under non-paddy and paddy management. Data are the mean values of three replicates with standard errors.

Soil/Horizon	Fe_o[a] ($g\ kg^{-1}$)	Mn_o[a] ($g\ kg^{-1}$)	Al_o[a] ($g\ kg^{-1}$)	Fe_d[b] ($g\ kg^{-1}$)	Mn_d[b] ($g\ kg^{-1}$)	Fe_c[c]	Fe_o/Fe_d	Mn_o/Mn_d
Non-paddy								
Ap1	4.00 ± 0.12	0.10 ± 0.01	1.01 ± 0.05	8.13 ± 0.05	0.12 ± 0.01	4.13	0.49	0.80
Ap2	4.00 ± 0.14	0.10 ± 0.01	0.97 ± 0.03	8.33 ± 0.08	0.13 ± 0.01	4.33	0.48	0.73
Bgw	2.16 ± 0.12	0.07 ± 0.02	0.64 ± 0.03	7.28 ± 0.32	0.08 ± 0.02	5.12	0.30	0.77
2Bgw	1.04 ± 0.06	0.14 ± 0.02	0.59 ± 0.06	9.84 ± 0.39	0.16 ± 0.03	8.80	0.11	0.87
3C	1.08 ± 0.05	0.18 ± 0.01	0.52 ± 0.07	5.16 ± 0.25	0.20 ± 0.01	4.08	0.21	0.91
Paddy								
Arp1	1.86 ± 0.03	0.01 ± 0.01	0.71 ± 0.03	3.40 ± 0.11	0.06 ± 0.01	1.53	0.55	0.12
Arp2	2.03 ± 0.03	0.01 ± 0.01	0.73 ± 0.01	3.31 ± 0.20	0.06 ± 0.01	1.27	0.61	0.12
Arpd	4.04 ± 0.93	0.01 ± 0.01	0.72 ± 0.03	6.98 ± 1.64	0.07 ± 0.01	2.94	0.58	0.18
Brd1	7.96 ± 0.84	0.14 ± 0.01	0.97 ± 0.12	17.95 ± 2.46	0.15 ± 0.05	9.99	0.44	0.97
Brd2	6.22 ± 0.35	1.67 ± 0..24	1.20 ± 0.09	12.35 ± 0.33	1.99 ± 0.22	6.13	0.50	0.84
Bg1	5.61 ± 0.36	0.34 ± 0.09	1.27 ± 0.18	11.00 ± 0.36	0.33 ± 0.06	5.39	0.51	1.03
Bg2	4.25 ± 1.75	0.27 ± 0.10	2.04 ± 0.24	8.41 ± 1.78	0.27 ± 0.11	4.17	0.50	0.99
2CBw	1.79 ± 0.37	0.09 ± 0.06	2.46 ± 0.28	4.58 ± 0.55	0.23 ± 0.09	2.79	0.39	0.40
3C	0.63 ± 0.20	0.21 ± 0.05	1.74 ± 0.21	2.69 ± 0.58	0.20 ± 0.02	2.07	0.23	1.04

[a] NH_4-oxalate-extractable Fe, Mn and Al

[b] Dithionite-citrate-bicarbonate extractable Fe and Mn

[c] Crystalline Fe oxides calculated as the difference between Fe_d and Fe_o

Table 3. Concentrations of organic C (mg C l^{-1}) in water-dispersible fine colloids (WDFC) from soil horizons under non-paddy and paddy management, and distribution between colloidal size-fractions as a function of depth, and after *in vitro* incubation under anoxic conditions. Fractions F1, F2 and F3 correspond to a size range of < 30nm, 30-240 nm and > 240 nm, respectively. Fractions (%) with respect to total WDFC organic C of each soil are given in parentheses. Data are the mean values of three replicates with standard errors.

Soil/Horizon	WDFC (mg C l^{-1})	DOC (mg C l^{-1})[a]	F1 (mg C l^{-1})	F2 (mg C l^{-1})	F3 (mg C l^{-1})
Non-paddy					
Ap1	7.0 ± 0.4	3.1 ± 0.2	0.2 ± 0.0 (3)	0.5 ± 0.1 (7)	3.2 ± 0.4 (45)
Ap2	6.2 ± 0.2	1.9 ± 0.2	0.3 ± 0.0 (4)	0.5 ± 0.1 (7)	3.6 ± 0.2 (58)
Bgw	2.7 ± 0.4	1.0 ± 0.2	0.1 ± 0.0 (4)	0.2 ± 0.1 (6)	1.4 ± 0.3 (54)
3C	0.5 ± 0.1	0.1 ± 0.1	0.1 ± 0.0 (12)	0.1 ± 0.0 (22)	0.2 ± 0.1 (45)
after anoxic incubation					
Ap1	19.0 ± 1.1	6.8 ± 0.6	1.1 ± 0.1 (6)	2.7 ± 0.7 (14)	8.4 ± 0.9 (44)
Ap2	17.2 ± 0.8	7.1 ± 0.3	1.4 ± 0.0 (8)	1.6 ± 0.2 (9)	7.1 ± 0.5 (41)
Paddy					
Arp1	4.3 ± 0.5	1.8 ± 0.2	0.1 ± 0.0 (3)	0.2 ± 0.0 (4)	2.2 ± 0.4 (51)
Arp2	3.1 ± 0.4	1.7 ± 0.4	0.1 ± 0.0 (2)	0.1 ± 0.0 (2)	1.3 ± 0.2 (42)
Arpd	3.9 ± 0.4	1.5 ± 0.1	0.1 ± 0.0 (2)	0.3 ± 0.1 (6)	2.1 ± 0.4 (53)
Brd1	9.4 ± 0.9	1.5 ± 0.2	0.1 ± 0.0 (2)	2.3 ± 0.4 (24)	5.4 ± 0.7 (57)
Brd2	7.5 ± 0.6	1.5 ± 0.1	0.1 ± 0.0 (2)	1.2 ± 0.2 (16)	4.7 ± 0.4 (62)
3C	1.7 ± 0.6	1.2 ± 0.6	0.1 ± 0.0 (9)	0.1 ± 0.0 (6)	0.3 ± 0.0 (21)
after anoxic incubation					
Arp1	13.0 ± 0.5	2.8 ± 1.1	1.9 ± 0.3 (14)	2.2 ± 0.3 (17)	6.2 ± 0.3 (48)
Arp2	12.0 ± 1.7	5.0 ± 1.5	1.4 ± 0.4 (11)	0.7 ± 0.1 (6)	4.9 ± 0.2 (43)

[a] Calculated as the difference between organic C in WDFC and the sum of organic C in the F1, F2 and F3 colloidal fractions

Table 4. Concentrations of Fe, Mn, Al and Si (mg l^{-1}) in colloidal size-fractions F2 and F3 of water-dispersible fine colloids (WDFC) obtained from soil horizons under non-paddy and paddy management as a function of depth, and after *in vitro* incubation under anoxic conditions. Fractions F2 and F3 correspond to a size range of 30-240 nm and > 240 nm, respectively. Concentrations in the fraction F1 (< 30 nm) were below the limits of detection. Data are the mean values of three replicates with standard errors.

Soil/Horizon	Fe (mg l^{-1})		Mn (mg l^{-1})		Al (mg l^{-1})		Si (mg l^{-1})	
	F2	F3	F2	F3	F2	F3	F2	F3
Non-paddy								
Ap1	9.0 ± 2.1	11.5 ± 0.7	0.1 ± 0.1	0.1 ± 0.1	13.3 ± 3.2	16.5 ± 1.4	31.3 ± 7.6	40.4 ± 3.6
Ap2	7.4 ± 1.2	11.0 ± 0.8	0.1 ± 0.1	0.1 ± 0.1	10.4 ± 1.6	15.6 ± 1.4	25.1 ± 3.6	38.4 ± 3.6
Bgw	2.7 ± 1.3	10.6 ± 2.2	n.d.	0.1 ± 0.1	4.1 ± 1.8	17.5 ± 2.9	9.3 ± 4.3	38.7 ± 6.5
3C	n.d.	0.2 ± 0.1	n.d.	n.d.	n.d.	0.7 ± 0.6	0.1 ± 0.1	1.5 ± 1.2
after anoxic incubation								
Ap1	48.1 ± 0.6	55.9 ± 1.9	0.2 ± 0.1	0.3 ± 0.1	59.7 ± 0.8	68.7 ± 1.6	64.5 ± 1.0	77.5 ± 1.7
Ap2	39.6 ± 6.2	49.5 ± 1.5	0.1 ± 0.1	0.2 ± 0.1	48.1 ± 6.7	61.3 ± 1.0	52.8 ± 7.5	69.3 ± 1.1
Paddy								
Arp1	3.0 ± 1.1	5.2 ± 0.5	n.d.	n.d.	7.6 ± 2.6	11.8 ± 0.8	18.9 ± 6.4	30.0 ± 2.1
Arp2	3.4 ± 1.2	4.5 ± 0.6	n.d.	n.d.	8.6 ± 3.0	10.0 ± 1.1	21.2 ± 7.2	25.3 ± 2.8
Arpd	3.6 ± 1.4	9.2 ± 4.0	n.d.	n.d.	6.1 ± 1.0	15.0 ± 4.3	14.7 ± 2.1	36.7 ± 10.3
Brd1	70.6 ± 8.4	32.5 ± 3.8	0.4 ± 0.1	0.2 ± 0.1	78.9 ± 7.3	31.6 ± 3.3	178 ± 16	72.7 ± 6.9
Brd2	39.2 ± 4.5	24.0 ± 2.4	0.6 ± 0.1	0.5 ± 0.1	69.1 ± 7.3	37.5 ± 5.5	155 ± 16	84.3 ± 12.2
3C	0.1 ± 0.1	0.2 ± 0.1	n.d.	n.d.	0.1 ± 0.1	0.3 ± 0.1	0.2 ± 0.1	0.9 ± 0.2
after anoxic incubation								
Arp1	17.1 ± 1.7	19.8 ± 1.3	n.d.	0.1 ± 0.1	30.5 ± 3.0	35.2 ± 1.6	35.8 ± 3.6	41.9 ± 1.7
Arp2	11.4 ± 1.0	21.1 ± 0.5	n.d.	0.1 ± 0.1	18.5 ± 3.7	34.6 ± 1.9	22.0 ± 4.2	41.7 ± 1.9

n.d., not detected

Table 5. Element molar ratios in colloidal size-fractions F2 and F3 of water-dispersible fine colloids (WDFC) obtained from soil horizons under non-paddy and paddy management as a function of depth, and after *in vitro* incubation under anoxic conditions. Fractions F2 and F3 correspond to a size range of 30-240 nm and > 240 nm, respectively. Data are the mean values of three replicates.

Soil/Horizon	C/Fe		Fe/Al		Fe/Si		Si/Al	
	F2	F3	F2	F3	F2	F3	F2	F3
Non-paddy								
Ap1	0.31	1.36	0.33	0.34	0.14	0.14	2.28	2.35
Ap2	0.33	1.65	0.34	0.34	0.15	0.14	2.33	2.37
Bgw	0.63	0.68	0.30	0.29	0.14	0.13	2.16	2.14
3C	n.d.	n.d.	n.d.	0.15	n.d.	0.06	n.d.	2.42
after anoxic incubation								
Ap1	0.23	0.80	0.39	0.39	0.37	0.36	1.04	1.09
Ap2	0.22	0.74	0.39	0.39	0.37	0.36	1.06	1.09
Paddy								
Arp1	0.35	2.04	0.19	0.21	0.08	0.09	2.40	2.46
Arp2	0.14	1.44	0.19	0.22	0.08	0.09	2.39	2.43
Arpd	0.32	1.24	0.26	0.27	0.11	0.12	2.33	2.37
Brd1	0.20	0.91	0.43	0.49	0.20	0.22	2.18	2.22
Brd2	0.15	0.97	0.27	0.31	0.13	0.14	2.16	2.17
3C	n.d.	n.d.	0.49	0.31	0.19	0.13	2.86	2.45
after anoxic incubation								
Arp1	0.62	1.51	0.27	0.27	0.24	0.24	1.13	1.15
Arp2	0.30	1.10	0.28	0.28	0.25	0.24	1.14	1.15

n.d. not determined

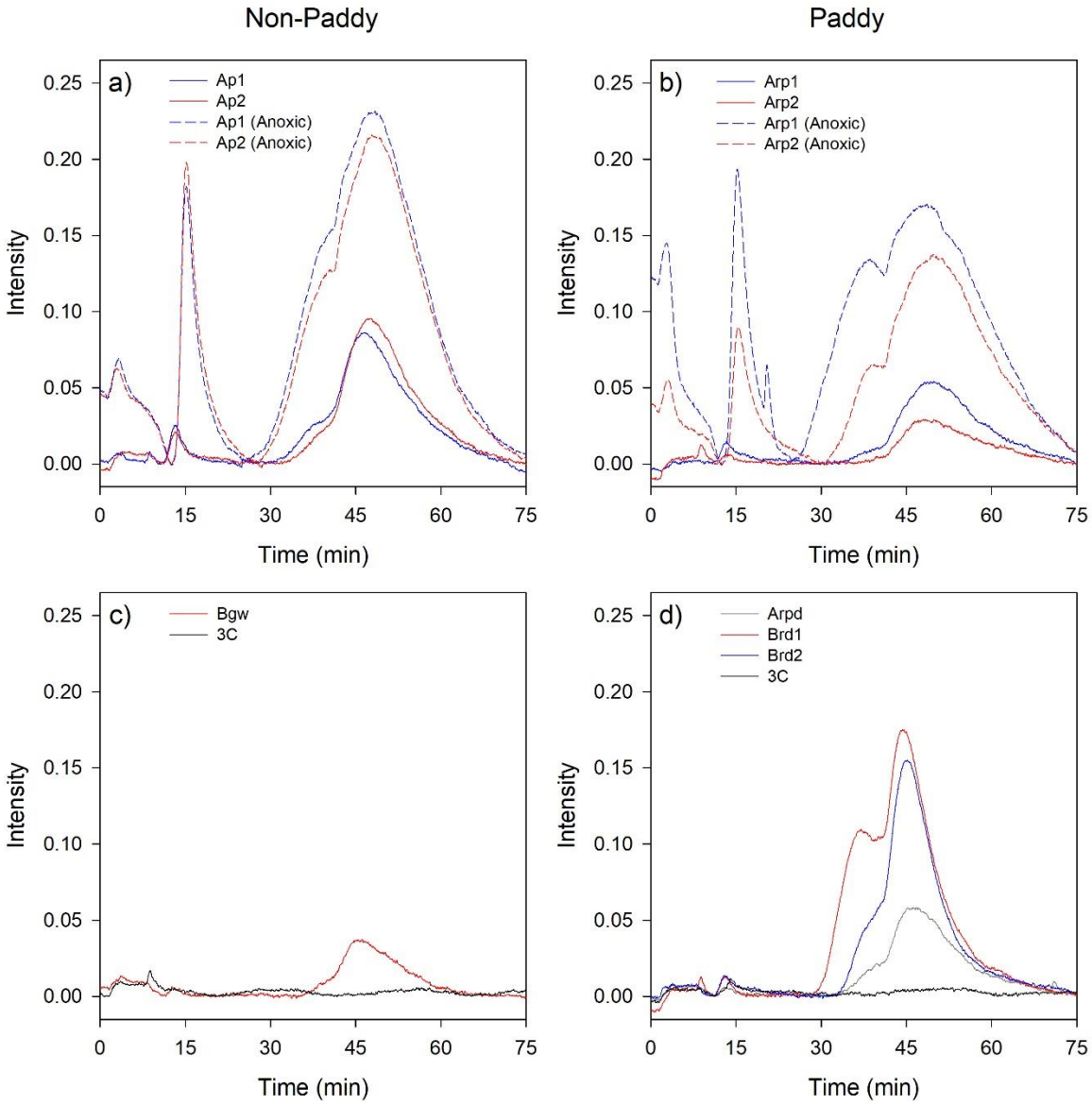

Figure 1. Asymmetric flow field-flow fractionation (AF4) organic C fractograms of water-dispersible fine colloids (WDFC) extracted from superficial (a, b) and sub-superficial (c, d) horizons under non-paddy (a, c) and paddy (b, c) management. Dashed lines in (a) and (b) represent the organic C fractograms of WDFC extracted from superficial soil samples after *in vitro* incubation under anoxic conditions.

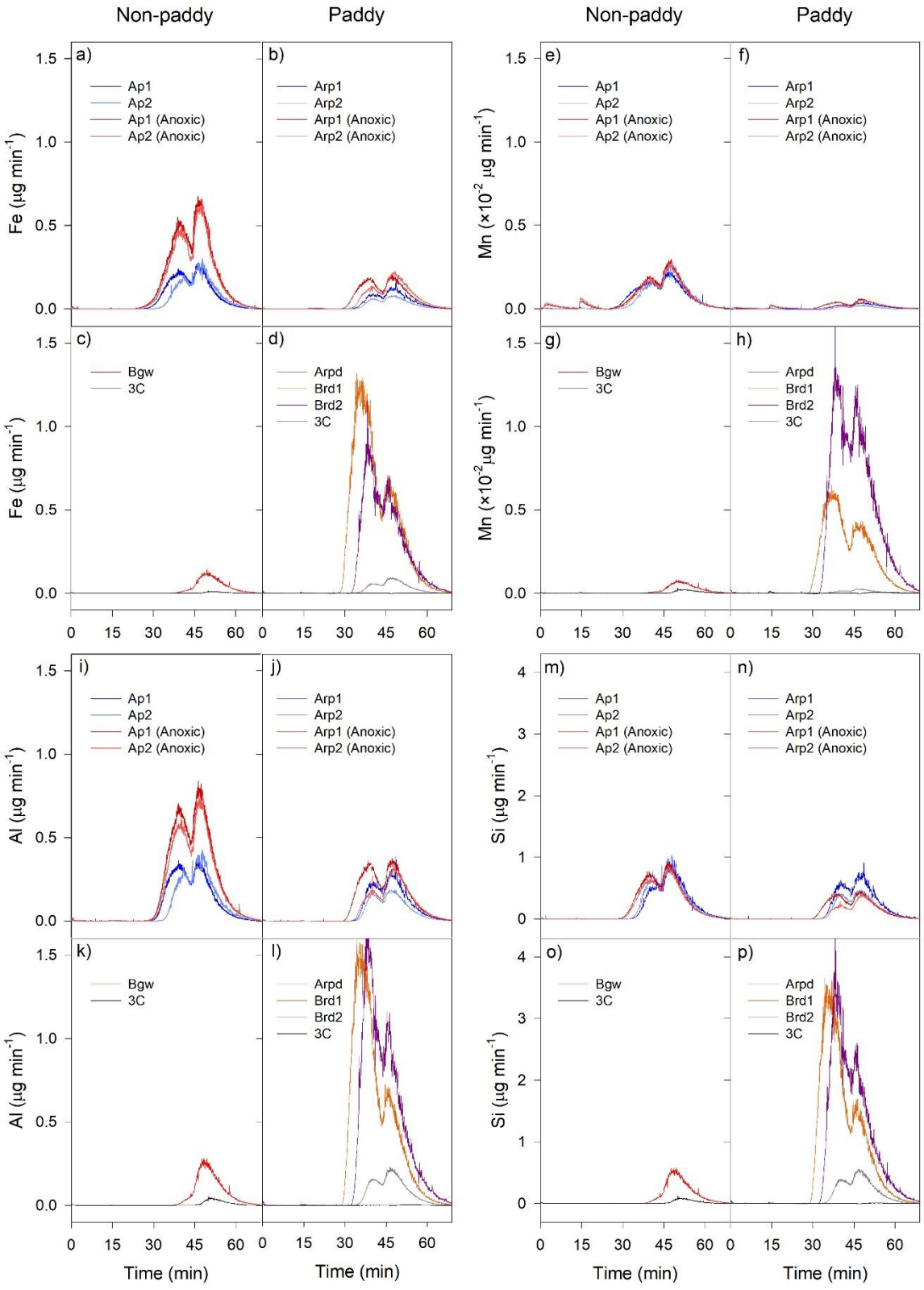

Figure 2. Asymmetric flow field-flow fractionation (AF4) fractograms of water-dispersible fine colloids (WDFC) extracted from superficial (a, b, e, f, i, j, o, p) and sub-superficial (c, d, g, h, k, l, o, p) horizons under non-paddy (a, c, e, g, i, k, m, o) and paddy (b, d, f, h, j, l, n, p) management, showing Al, Si, Fe and Mn mass flow monitored by inductively coupled plasma mass spectrometry. "Anoxic"-labelled series in superficial horizons (a, b, e, f, i, j, o, p) represent the fractograms of WDFC extracted from superficial soil samples after *in vitro* incubation under anoxic conditions.

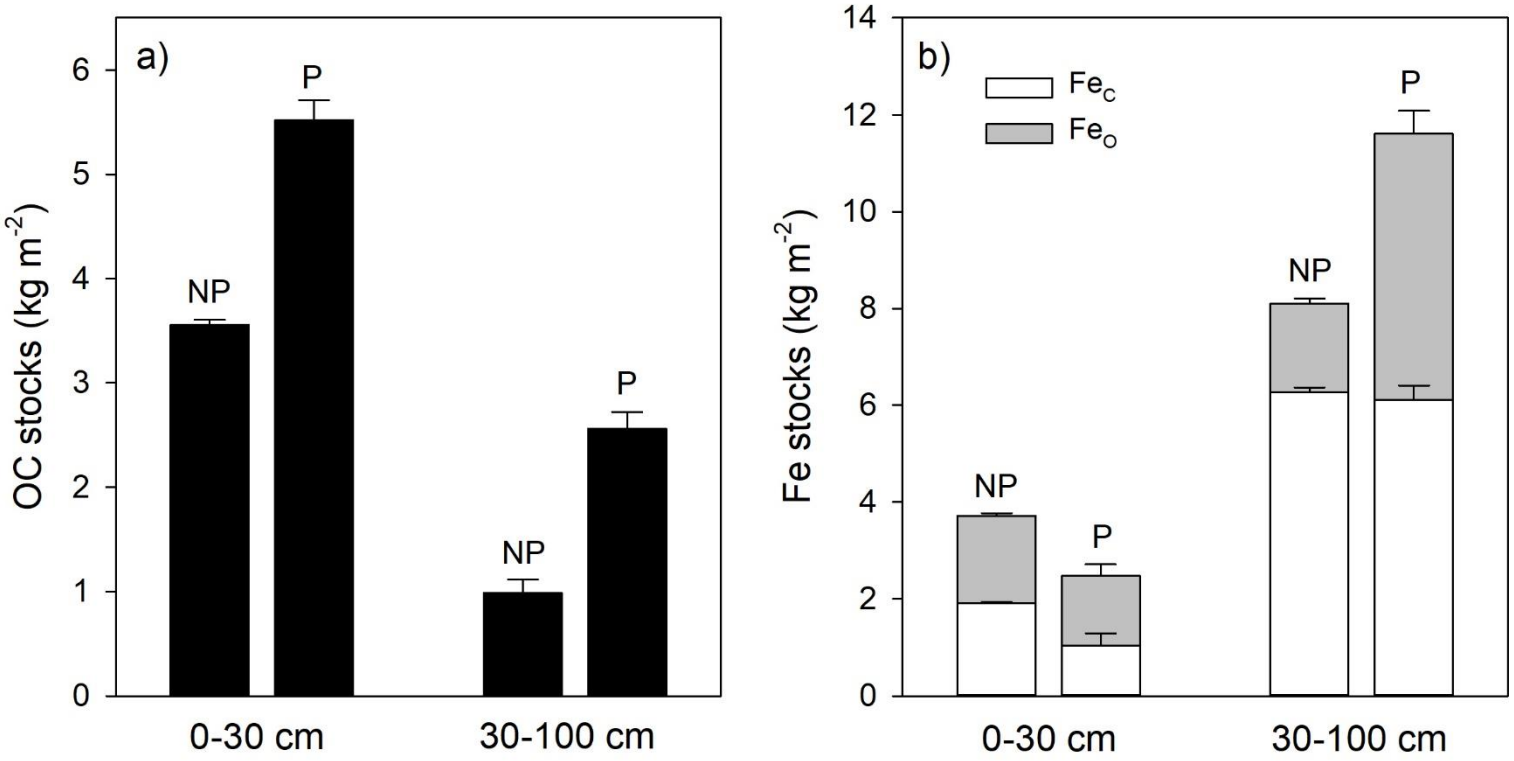

Figure 3. Organic C (a), and short-range ordered (Fe_o) and crystalline (Fe_c) Fe oxide (b) stocks in topsoil (0-30 cm) and subsoil (30-100 cm) horizons under non-paddy (NP) and paddy (P) management. Error bars represent standard error.

Graphical Abstract

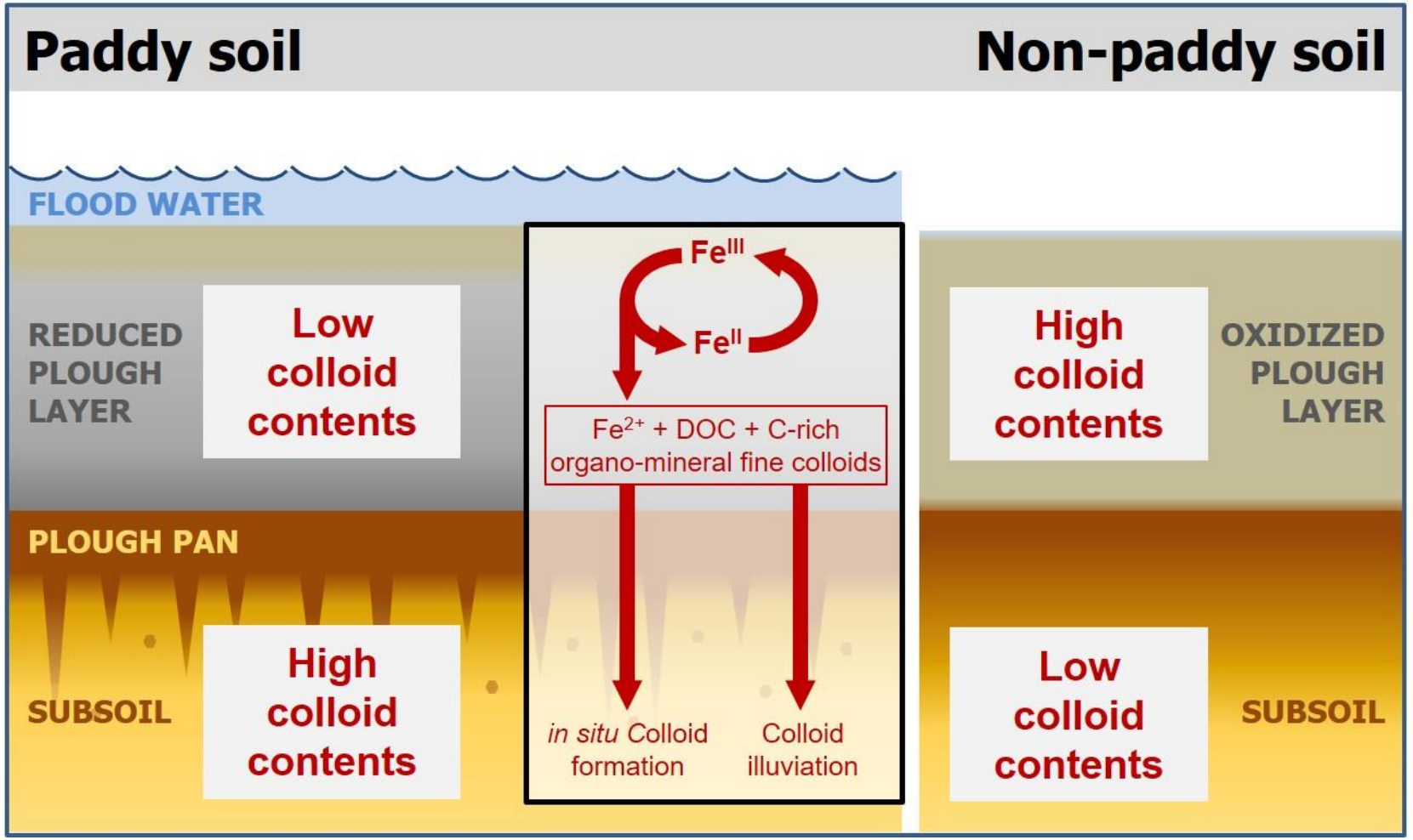

Redox-driven changes in water-dispersible colloids and their role in carbon cycling in hydromorphic soils

Daniel Said-Pullicino[1], Beatrice Giannetta[1], Beatrice Demeglio[1], Anna Missong[2], Nina Gottselig[3], Marco Romani[4], Roland Bol[2], Erwin Klumpp[2], Luisella Celi[1]

[1]*Soil Biogeochemistry, Department of Agricultural, Forest and Food Sciences, University of Torino, Grugliasco (TO), Italy.*

[2]*Institute of Bio- and Geosciences, Agrosphere Institute (IBG-3), Forschungszentrum Jülich, Germany.*

[3]*Soil Science and Soil Ecology, Institute of Crop Science and Resource Conservation, Universität Bonn, Germany.*

[4]*Rice Research Centre, Ente Nazionale Risi, Castello d'Agogna, Italy.*

Supplementary Material

Soil samples from the topsoil horizons from the non-paddy (Ap1 and Ap2) and paddy soil (Arp1 and Arp2) were incubated under anoxic conditions in the dark at 20 °C for 35 days prior to isolating water-dispersible fine colloids (WDFC) for characterization by asymmetric flow field-flow fractionation (AF4). During the incubation, a separate set of vials were destructively sampled to follow the changes in pH, Eh and soil solution concentrations of Fe^{2+} and DOC. Soil slurries were prepared by suspending 20 g of air dried soil aliquots in 50 ml of degassed ultrapure water in crimp-top vials that were sealed and flushed with N_2 to ensure anaerobic conditions. Vials for each soil were harvested in triplicate after 1, 7, 14, 21, 28 and 35 d from the start of the incubation. On the day of sampling, pH and Eh were measured were measured potentiometrically in the soil slurry, while Fe^{2+} and DOC concentrations were quantified in the soil solution after filtration (0.45 μm nylon membrane filter) in the anaerobic glovebox. Dissolved Fe(II) concentrations were measured colorimetrically using the 1,10-phenanthroline method. Dissolved organic carbon was determined using Pt-catalyzed, high-temperature combustion (850 °C) followed by infrared detection of CO_2 (VarioTOC, Elementar, Hanau, Germany), after removing inorganic C by acidifying to pH 2 and purging with CO_2-free synthetic air. Changes in these parameters during the incubation period are reported in Fig. S1.

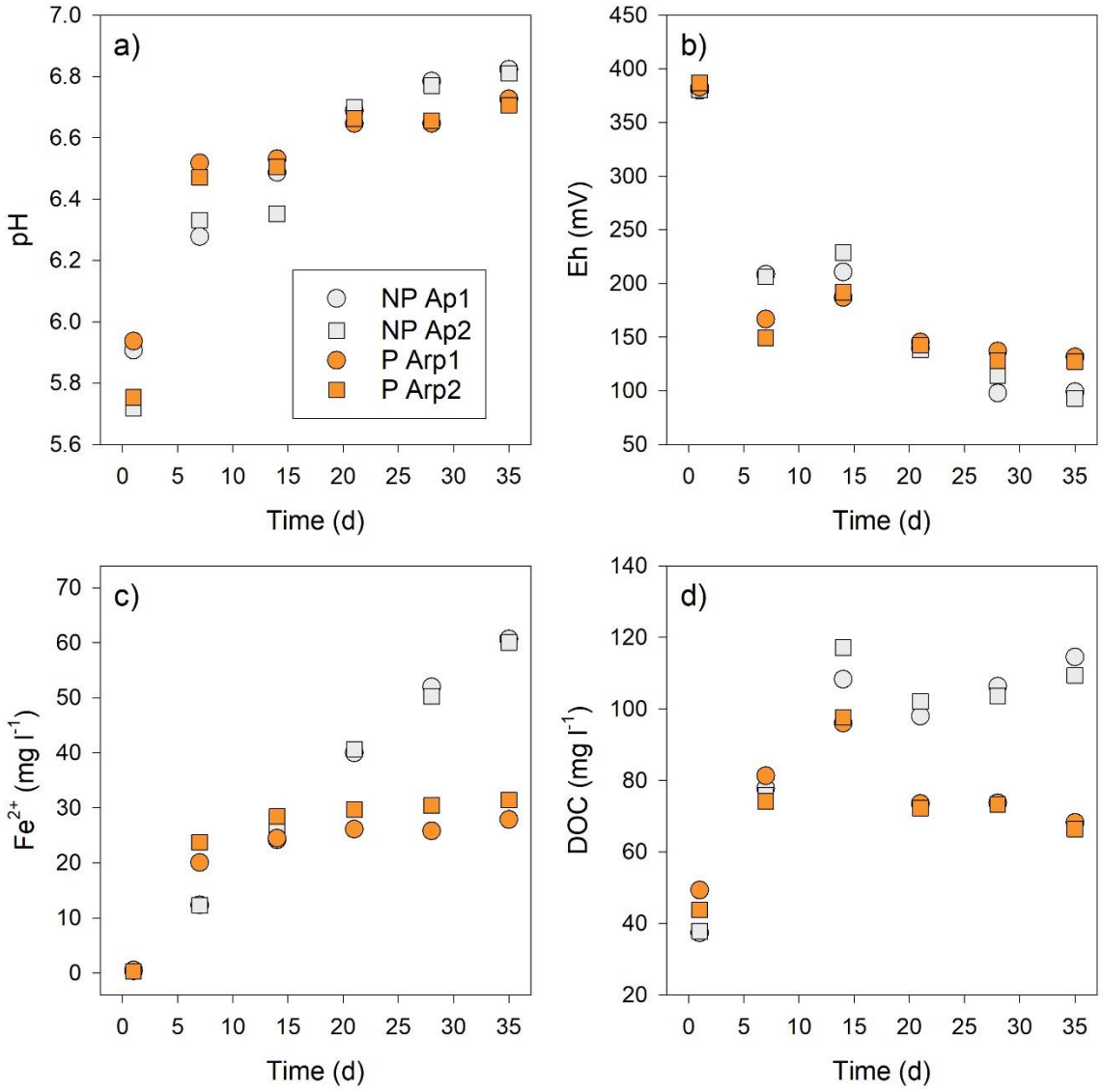

Figure S1. Changes in (a) pH, (b) Eh, (c) dissolved Fe^{2+} and (d) DOC during the anaerobic incubation of paddy (P) and non-paddy (NP) topsoils.